RAA 2019 Vol. **19** No. **10**, 149(14pp) doi: 10.1088/1674–4527/19/10/149

http://www.raa-journal.org *http://iopscience.iop.org/raa*

Research in Astronomy and Astrophysics

Lijiang 2.4-meter Telescope and its instruments

Chuan-Jun Wang[1,2,3,4], Jin-Ming Bai[1,2,3], Yu-Feng Fan[1,2,3], Ji-Rong Mao[1,2,3], Liang Chang[1,2,3,4], Yu-Xin Xin[1,2,3,4], Ju-Jia Zhang[1,2,3], Bao-Li Lun[1,2,3], Jian-Guo Wang[1,2,3], Xi-Liang Zhang[1,2,3], Mei Ying[5], Kai-Xing Lu[1,2,3], Xiao-Li Wang[1,2,3], Kai-Fan Ji[1,3], Ding-Rong Xiong[1,2,3], Xiao-Guang Yu[1,2,3], Xu Ding[1,2,3], Kai Ye[1,2,3], Li-Feng Xing[1,2,3], Wei-Min Yi[1,2,3], Liang Xu[1,2,3], Xiang-Ming Zheng[1,2,3], Yuan-Jie Feng[1,2,3], Shou-Sheng He[1,2,3], Xue-Li Wang[1], Zhong Liu[1], Dong Chen[1], Jun Xu[1], Song-Nian Qin[1], Rui-Long Zhang[1], Hui-Song Tan[1], Zhi Li[1], Ke Lou[1], Jian Li[1] and Wei-Wei Liu[1]

[1] Yunnan Observatories, Chinese Academy of Sciences, Kunming 650216, China; *wcj@ynao.ac.cn, baijinming@ynao.ac.cn*

[2] Key Laboratory for the Structure and Evolution of Celestial Objects, Chinese Academy of Sciences, Kunming 650216, China

[3] Center for Astronomical Mega-Science, Chinese Academy of Sciences, Beijing 100101, China

[4] University of Chinese Academy of Sciences, Beijing 100049, China

[5] Astrophysics Center of Guangzhou University, Guangzhou 510006, China

Received 2018 November 29; accepted 2019 May 14

Abstract The Lijiang 2.4-meter Telescope (LJT), the largest common-purpose optical telescope in China, has been available to the worldwide astronomical community since 2008. It is located at the Gaomeigu site, Lijiang Observatory (LJO), in the southwest of China. The site has very good observational conditions. During its 10-year operation, several instruments have been equipped on the LJT. Astronomers can perform both photometric and spectral observations. The main scientific goals of LJT include recording photometric and spectral evolution of supernovae, reverberation mapping of active galactic nuclei, investigating the physical properties of binary stars and near-earth objects (comets and asteroids), and identification of exoplanets and all kinds of transients. Until now, the masses of 41 high accretion rate black holes have been measured, and more than 168 supernovae have been identified by the LJT. More than 190 papers related to the LJT have been published. In this paper, the general observation conditions of the Gaomeigu site is introduced at first. Then, the structure of the LJT is described in detail, including the optical, mechanical, motion and control system. The specification of all the instruments and some detailed parameters of the YFOSC is also presented. Finally, some important scientific results and future expectations are summarized.

Key words: telescopes: Lijiang 2.4-m Telescope — instrumentation: photometers — instrumentation: spectrographs

1 INTRODUCTION

The Lijiang 2.4-meter Telescope is operated by Lijiang Observatory (IAU code O44), Yunnan Observatories (YNAO), Chinese Academy of Sciences (CAS). The location of the observatory is $100°1'48''$(E), $26°41'42''$(N), with an altitude of 3193 meters (Fig. 1). The observational conditions of the site are summarized in Table 1 (Xin et al. 2017). A site survey for the 2.4-meter telescope began in 1994, and the construction of the Lijiang 2.4-meter Telescope as well as the Lijiang Observatory began in 2003. The telescope was being tested with instruments installed from 2008, and it has been available to astronomers for astronomical observations since 2012.

The Lijiang 2.4-meter telescope is the largest optical telescope at present in China for general astronomical observation. It can play more and more important roles in the future. The telescope was designed by the Telescope Technology Limited (TTL) company in Liverpool, England, and it provides very stable and precise performance. This telescope has a traditional altitude-azimuth mount that holds a Ritchey-Chrétien Cassegrain optical design. The main body of the telescope is under a truss structure and supported by a hydrostatic bear-

Table 1 Observation Conditions of Lijiang Observatory

Average Observation Time (hours)	2150 (2012 to 2014)	2000 (2015 to 2017)
Sky Brightness	V:22.06 mag/sq.arcsec	22.14 mag/sq.arcsec
Extinction Coefficient	KV=0.14	KB=0.3
Seeing (Average)	$0.97''$(2014)	$1.0''$(2015)

Notes: We utilize the Sky Quality Meter (SQM-LE) produced by the Unihedron Company to measure the nighttime sky brightness.

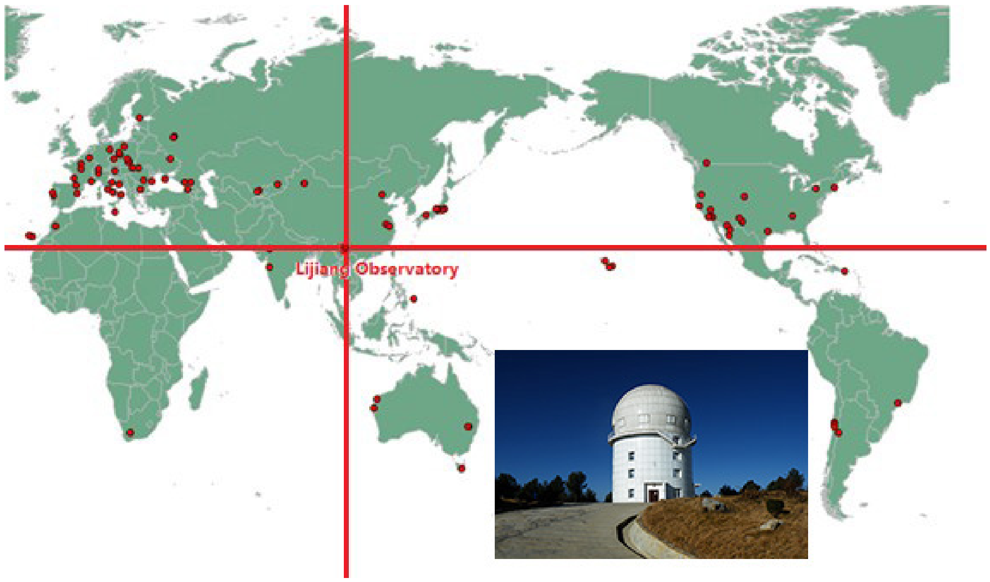

Fig. 1 Location of Lijiang Observatory and 2.4-meter telescope dome.

ing system. The primary mirror is supported both axially and laterally by a three-sector pneumatic support system. The telescope incorporates a real-time motion control system that enables accurate position in altitude, azimuth and Cassegrain axes of rotation. Additionally, the auto-guider selects star image centroids in the field-of-view (FOV) to provide refined tracking corrections to the control system. The pointing accuracy of this telescope is better than 2 arcsec, the open-loop tracking accuracy is better than 2 arcsec h^{-1} and the closed-loop tracking accuracy is better than 0.5 arcsec h^{-1}. The telescope and dome can be controlled automatically with embedded industrial PCs and a real-time operating system, that provide the possibility for remote and autonomous observation. The structure of the telescope is illustrated in Figure 2.

Although the telescope is small compared to other large telescopes around the world, many kinds of scientific investigations can still be carried out due to the important geographical location of the site. It can take photometric observations with standard Johnson and SDSS filters. Both low/medium and high-resolution spectral observations can be also performed. The main scientific goals of the telescope focus on time-domain astronomy, including photometric and spectroscopic evolution of supernovae, reverberation mapping of active galactic nuclei (AGN), physical properties of binary stars and near-earth objects (comets and asteroids), identification of exoplanets, gamma-ray burst follow-up, and gravitational wave electromagnetic counterpart observation. In addition, some other scientific issues, such as high-redshift quasars, Li-rich stars and precise CCD position of natural satellites of planets in the solar system, are also included. The instruments mounted on the telescope are the Yunnan Faint Object Spectrograph and Camera (YFOSC), Li-Jiang Exoplanet Tracker (LiJET), High Resolution Spectrograph (HiRES), Multicolor Photometric System (PI CCD) and China Lijiang Integral Field Unit (CHILI). Thanks to the Rapid Instrument Exchanging System that we installed in 2012, observers can switch to a certain instrument quickly and perform semi-simultaneous photometric and spectral observations of the same target. Thus, the telescope can acquire several kinds of observations during a single night (Fan et al. 2015).

We describe the structure of the 2.4-meter telescope in detail, including optical, mechanical, motion and control systems, in Section 2. The instruments attached to the telescope are introduced in Section 3. Some important equipment related to the telescope are presented in Section 4. Some observational outputs of the telescope are summa-

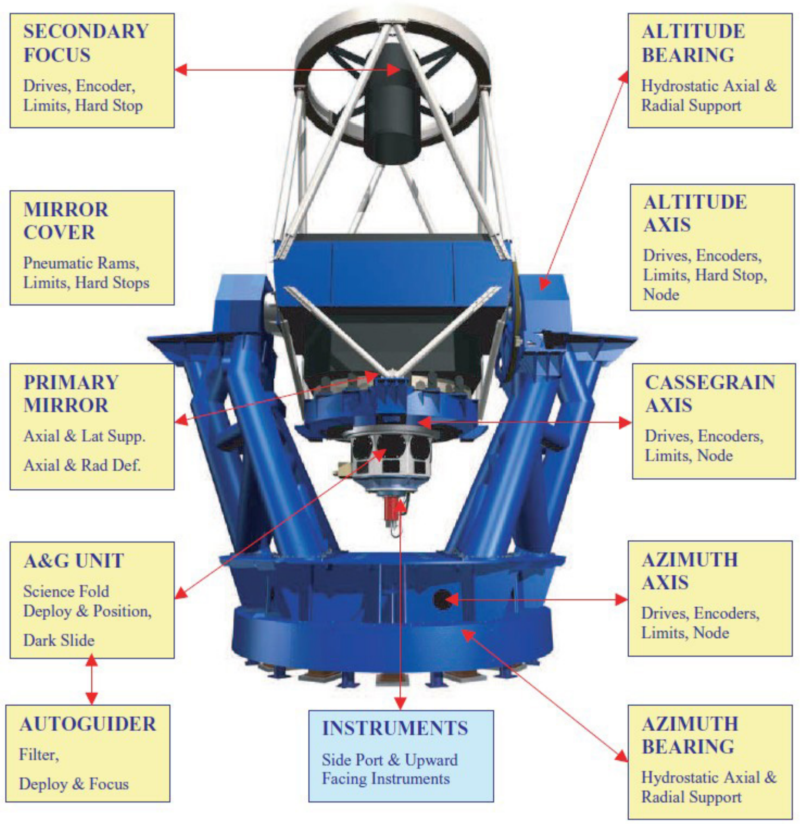

Fig. 2 The 2.4-meter telescope system.

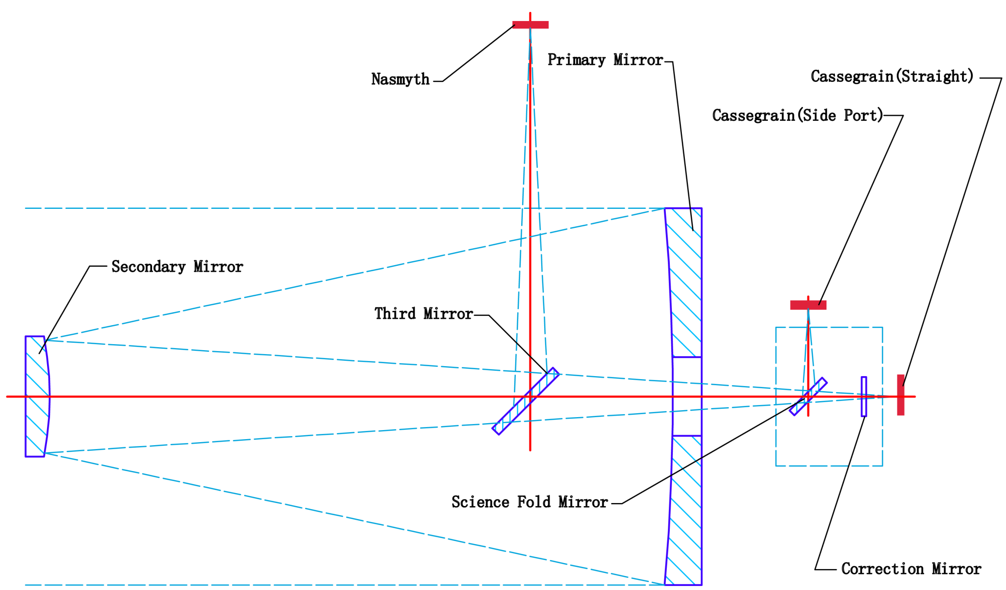

Fig. 3 Optical diagram for the 2.4-meter telescope.

rized in Section 5. Some expected progresses in the future are reported in Section 6.

2 STRUCTURE OF 2.4-METER TELESCOPE

The 2.4-meter telescope is comprised of four main subsystems. They are the optical system, mechanical system, mo-

Table 2 Telescope Optical Specification

Primary Mirror	Clear Aperture	2400 mm
	Central Bore	500 mm
	Focal Ratio	F/2.43
	Radius of Curvature	–11520 mm
	Conic Constant	–1.073
Secondary Mirror	Clear Aperture	709 mm
	Radius of Curvature	–4760.44 mm
	Conic Constant	–4.187
	Distance to Primary Mirror	4094.114 mm
	Distance to Focal Plane	5550.870 mm
Cassegrain focus	Focal Ratio	F/8
	FOV of Fold Port	8 arcmin
	FOV of Straight Port	10 arcmin
	Corrected FOV of Straight Port	40 arcmin
Nasmyth focus	Focal Ratio	F/8
	FOV	8 arc min

tion system and control system. All of them are described in detail in the following subsections.

2.1 Optical System

The optical design of the primary and secondary mirrors is a Ritchey-Chrétien Cassegrain structure, which provides one Cassegrain focus and two Nasmyth foci. The on-axis FOV of the Cassegrain focus is 10 arcmin, and it can reach 40 arcmin by employing a correction mirror. By utilizing a $45°$ folding mirror installed in the A&G box at the Cassegrain, we can obtain one straight port and eight side ports at the Cassegrain focal station. Thus, we can install nine instruments on the telescope at the same time. The Nasmyth focal station can be switched by setting the third mirror into the tube that is mounted from the telescope center section. The Nasmyth focal station can provide an FOV of 8 arcmin. The telescope image is kept in focus by moving the secondary mirror axially. The optical specifications of the telescope are listed in Table 2, and the optical diagram of the telescope is illustrated in Figure 3 (also see Fan et al. 2015).

The concave primary mirror is made of Zerodur, a glass-ceramic material with a nearly zero thermal coefficient of expansion. It is coated with aluminum. The back of the primary mirror is flat. This is convenient for the axial support pads that bear weight during operation but are not physically attached. Invar pads are bonded to the outer edge of the mirror for attaching both the lateral support system and the mirror defining system. The primary mirror is depicted in the left panel of Figure 4. The convex secondary mirror is also made of Zerodur. The back of it is flat with a central bore. Invar pads are bonded to the back surface of the mirror for attaching the axial support system, while the lateral support is bonded inside the rear borehole. The secondary mirror is shown in the right panel of Figure 4.

There are two light baffles mounted on the telescope structure to prevent stray light from entering the focus of the telescope. The upper baffle is mounted from the secondary mirror assembly, and the lower baffle is mounted from the telescope center section. They are illustrated in Figure 5. The central beam obscuration is mainly caused by the secondary assembly. The supporting vanes of the secondary mirror and the lower baffle induce a small amount of additional obscuration. The total obscuration is 16.67%.

2.2 Mechanical System

The main body of the telescope is fabricated from a steel plate and steel tube, which are welded to have a high stiffness and low mass structure. The azimuth and altitude axes are supported by hydrostatic bearings. The azimuth axis takes three load bearings and three guide pads, and the altitude axis is supported by four load bearings and two guide bearings.

The telescope tube is the structure that carries the principal optical components of the telescope. The optical axis of the tube, defined by the Cassegrain rotation bearing, is arranged to intersect and be orthogonal with the altitude axis of rotation. The center section is the foundation of the telescope tube, which has two trunnion bearings attached at the two opposite sides using hydrostatic bearing pads to support the entire telescope tube. The tube is a traditional open-truss Serrurier construction that can maintain the optical alignment. The lower tube structure connects the center section with the primary mirror and the Cassegrain assembly. The upper tube structure is connected to the secondary mirror assembly. The mirror cover is mounted from the upper surface of the center section and it can be controlled by high-pressure air. The lower baffle is also mounted from the center section. We can mount a tertiary mirror at a 45 degree angle to the main light path

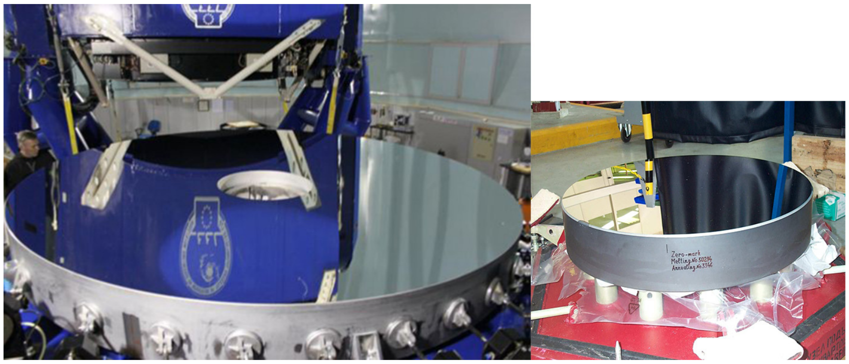

Fig. 4 The primary and secondary mirror.

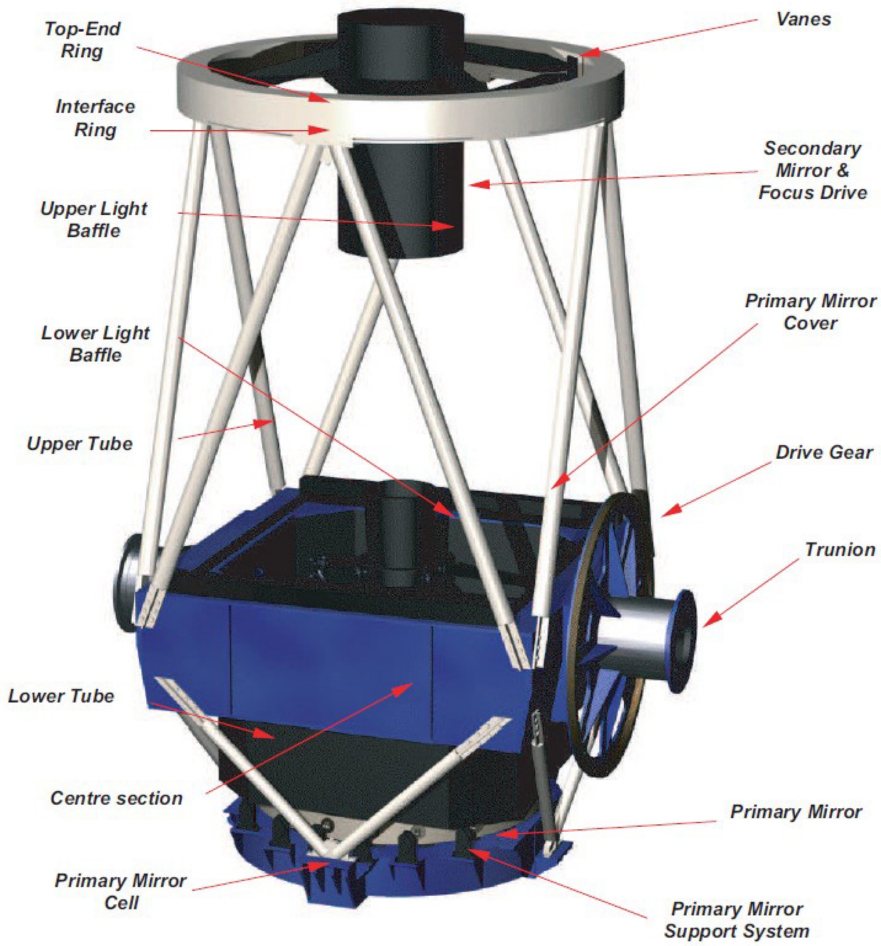

Fig. 5 The mechanical structure of the telescope tube.

of the telescope to direct the light to the Nasmyth focal station.

The primary mirror cell assembly provids a platform for the primary mirror support system, the Cassegrain rotator bearing and the Cassegrain rotator cable wrap. The structure of the primary cell is designed with a stiff-under structure to minimize distortions between the truss locations and the Cassegrain rotator bearing. The 2.3-ton primary mirror is supported by pneumatic actuators both axially and laterally. The axial units are divided into three sectors. Each sector has an axial-defining unit situated in the middle of it, and mounted at the outside edge of the mirror. A load cell in these units provides force feedback information for the mirror support system, which can be used to

Table 3 Parameters of CCD for YFOSC

Parameter	Value
Pixels	2048×4608
Pixel Size	13.5 μm×13.5 μm
Image Area	27.6 mm×62.2 mm
FOV	$9.60' \times 9.60'$
(Photometry)	(2K×2K)
Image Scale	$0.283''$/pixel
Cooling Mode	Liquid Nitrogen: –120°C
Gain	$0.33e^-$
Readout Noise	$6.3e^-$ (Speed: 400 kpixels s^{-1})
	$<5.0e^-$(Speed: 200 kpixels s^{-1})

correct any detected load by adjusting the air pressure in the axial actuators of the appropriate sector.

The top-end ring incorporates the interface ring and the upper telescope tube. It is used to support the secondary mirror cell. It is connected to the center section by the top interface. The secondary mirror cell can be disconnected from the interface ring without disturbing the alignment of the telescope tube.

The mechanical structure of the telescope tube is drawn in Figure 5.

2.3 Motion System

The motion system of the telescope incorporates all the motive elements, and is controlled by the Master Control System (MCS) from inputs supplied by the Telescope Control System (TCS) or the Engineering Control Interface (ECI). The motive elements include: azimuth, altitude, rotator, primary mirror support, mirror cover, secondary mirror focus assembly, auto-guider and science fold mirror. The main functions of the motion system are:

- Move the azimuth and altitude.
- Drive the secondary mirror focus.
- Drive the Cassegrain rotator.
- Support the primary mirror and drive the mirror cover.
- Deploy the auto-guider, move the auto-guider focus and deploy the filter.
- Deploy the science fold mirror and rotate it to the specified side port.

Both azimuth and altitude are driven by a pair of electric motors in the anti-backlash configuration. Each motor is connected to a gearbox and the outputs are used to drive a pinion. The position information is provided by a Heidenhain optical tape encoder adhered inside of the bearing, which can be transferred to the TCS.

In order to compensate the effect that the image on the focal plane rotates with the azimuth motion of the telescope when the telescope tracks a scientific target in azimuth and altitude, the Cassegrain rotator is used to derotate the image. The Cassegrain rotator is also driven by a pair of electric motors in an anti-backlash configuration, and the position information is also provided by the Heidenhain optical tape encoder.

2.4 Control System

The control system of the telescope can be divided into Safety Interlock System, Services System and Computing System.

Safety Interlock System: Independent Programmable Logic Controllers (PLCs) are employed to manage subordinate and supporting services for the telescope and enclosure. This system includes the control of interlocks between local and remote control. The control limit and emergency-stop (E-stop) can prevent major damage to the telescope structure, as well as electrical, pneumatic and optical systems. The whole telescope system will be shut down if one of the emergency-stops is triggered anywhere in the dome to protect the staff and science instruments.

Service System: Service system includes Enclosure PLC (EPLC) and Service PLC (SPLC). The EPLC mainly handles opening and closing the aperture, as well as tracking the target along with the telescope. The SPLC mainly handles all the auxiliary actions and services associated with the operation of the telescope. These actions include: electrical power control, electrical power distribution, local/remote control, control and monitoring of the hydrostatic bearing system, control and monitoring of the primary mirror support system, opening and closing the primary mirror cover, control and monitoring of the motion axis, controlling the telescope manually, on/off mount interlocking system, temperature monitoring, alarm handling, temperature monitoring of cooling system and local control.

Computing System: The computing system consists of several on-mount and off-mount industrial computers. The on-mount computers are Azimuth node, Altitude node, Cassegrain node, auxiliary mechanism node (AMN) and auto-guider control computer (ACC). The off-mount computers are Supervisory Control Computer (SCC, controls the start-up, shutdown and monitoring of all computing systems), Master Control Computer (MCC, to run the database that includes all telescope parameters, to operate the ECI and remote control, and monitor the enclosure), and Telescope Control Computer (TCC, to administer the TCS that can receive requirements or commands from the operator, and to perform astrometric transformation and send it back to MCS to perform the proper operation of the telescope). All on-mount and off-mount computers are connected to the telescope local area network, and all computers apart from the TCC employ the real-time operating system QNX. QNX is a network-wide operating system

Table 4 Parameters of major optical elements for YFOSC

			Size (μm)		Sky angle (″)		
Long Slit			54		0.58		
			74		0.8		
			93		1.0		
			112		1.2		
			140		1.5		
			168		1.8		
			233		2.5		
			470		5.0		
			940		10.0		
Short Slit			54 ×500		0.58 ×5.37		
			74 ×500		0.8 ×5.37		
			100 ×500		1.07 ×5.37		
			140 ×500		1.5 ×5.37		
			460 ×500		4.94 ×5.37		
			940 ×500		10.0 ×5.37		
Grism No.	λc (nm)	λ Blaze (nm)	Grooves (nm/mm)	Dispersion (nm/pix)	Resolution (@600nm/pix)	Sp. Range (nm)	Order Range
12	730	700	75	1.1	545	520–980	1
10	380	390	150	0.79	760	340–900	1
3	390	430	400	0.29	2068	340–910	1
15	586	527	300	0.39	1540	410–980	1
5	650	700	300	0.46	1300	496–980	1
14	463	428	600	0.17	3520	360–746	1
8	650	700	600	0.15	4000	510–960	1
13			316	0.06	10000	340–980	3, 4, 5
9			79	0.06	10000	340–980	7–23

Notes: We utilize the standard Johnson and SDSS filters for photometric observation, and the parameters of these filters are not listed in this table.

Table 5 Parameters of PI CCD

Parameter	Value
Pixels	1300×1340
Pixel Size	20 μm×20 μm
Image Area	26.0 mm×26.8 mm
FOV	4.40′×4.48′
Cooling Mode	Liquid Nitrogen: –70° C to –110° C, +/– 0.05° C
Linearity	< 1% (100 kHz), <2%(1 MHz)
Readout Noise	2.84e$^-$ (Low speed, Low noise mode)
	16.3e$^-$ (High speed, High gain mode)

Table 6 Parameters of CCD for HiRES

Parameter	Value
Pixels	4096×4096
Pixel Size	12 μm×12 μm
Image Area	49.2 mm×49.2 mm
Cooling Mode	TEC semiconductor cooling: –90° C (With water cycle cooling)
Readout Noise	<5.0e$^-$ (Readout speed: 50 kHz)
	<7.0e$^-$ (Readout speed: 250 kHz)

and provides an inherent network file system. Therefore, all on-mount computers are diskless nodes that can net-boot from the MCC during the startup period. After startup, all the on-mount computers apply the file system of MCC and SCC through the network.

3 INCORPORATED INSTRUMENTATION

There are five scientific instruments mounted on the Cassegrain focal station. They are YFOSC, PI CCD, HiRES, LiJET and CHILI. All of these instruments are described in detail in the following subsections.

3.1 YFOSC

YFOSC is the most popular instrument on the 2.4-meter telescope that is installed on the straight through port of the Cassegrain. It is a scientific instrument for multi-mode observation based on a focal reducer. It can perform photometry and low/medium dispersion spectral observations semi-synchronously. Time-domain observation is one of the major aims for the telescope, and we usually arrange different kinds of observations in one night. Thus, we need to switch observational modes frequently in a short time. We can easily use YFOSC to achieve different scientific aims by quickly switching observational modes. During the night, one observer can attempt different targets and perform different observations depending on the different observing conditions. It is convenient to change among different filters, grisms and slits. Its structure is depicted in Figure 6. It has five wheels: the aperture wheel, the YFUA and YFUB wheels, the filter wheel, and the grism wheel. All the wheels are controlled by an integrated control system that can change among different elements and perform different observations.

The CCD chip for YFOSC is a back illuminated type CCD chip produced by the e2v company. The CCD controller employs all-digital hyper-sampling technology

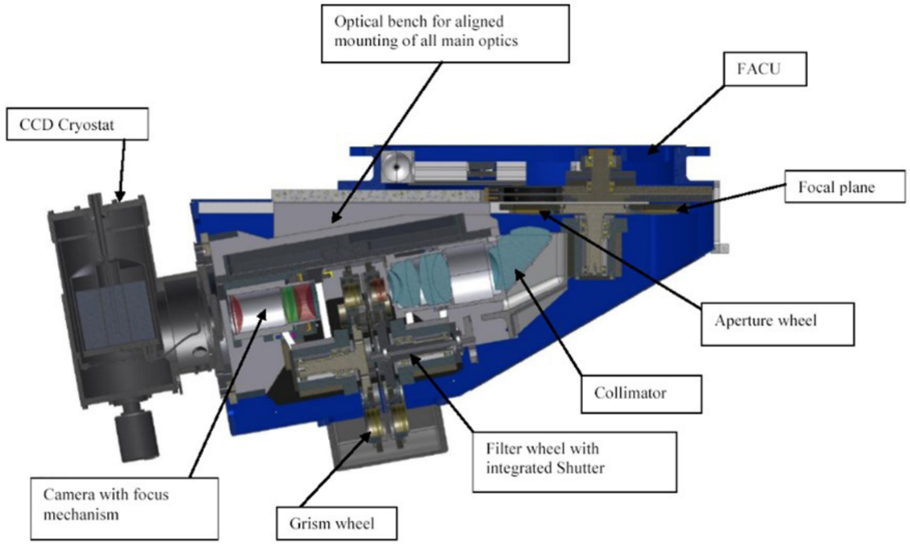

Fig. 6 The structure of YFOSC.

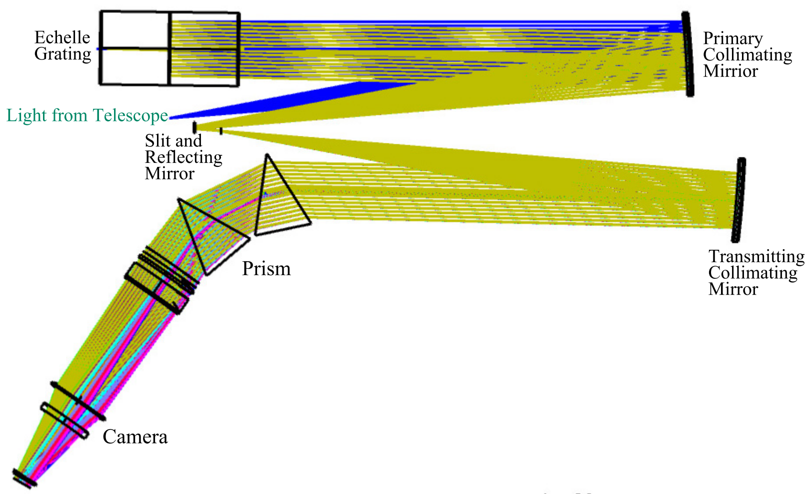

Fig. 7 The light path of HiRES.

called 3^{rd} generation CCDs (CCD3), which can ensure low readout noise with high readout speed. The parameters are listed in Table 3. All the optical elements installed onto YFOSC (except filters) are listed in Table 4.

For photometric observation, light goes through the collimating mirror, filters and imaging mirror. Then, the image is directed onto the CCD chip with a focus ratio conversion from F/8 to F4.1. This conversion can reduce the effect produced by oversampling the CCD and improve the ultimate detection capability. Using SDSS r-band filter with an exposure time of 20 minutes, the limiting magnitude of a point source is about 23.5 mag with the signal to noise ratio (S/N) $\geq$3 (Lun et al. 2014). Observers can reduce the readout section and use binning to reduce the readout time if necessary. When suitable aperture and grism are moved into the light path, YFOSC can change to spectral observing mode. YFOSC can record long-slit spectra and cross-dispersion spectra. Both kinds of spectra can cover wavelengths from 340 nm to 980 nm. The long-slit spectrum mode with a single grism can get a low-resolution spectrum. Using the long-slit spectrum with exposure time of 30 minutes, the limiting magnitude is 19.5 mag by 1.8$''$ aperture and the resolution is 300/pix with S/N ratio about 10. The target that attains this result is SN 2011fe (Zhang et al. 2016b). The cross-dispersion spectrum mode uses a low dispersion grism and medium dispersion echelle to record a medium resolution spectrum. The spectral resolution is 10 000 pix^{-1} under the magnitude limit of 15.5 mag by a 0.85$''$ aperture (Zhang et al. 2018b). The detailed spectral efficiency of each grism using a long slit was reported by Zhang et al. (2012).

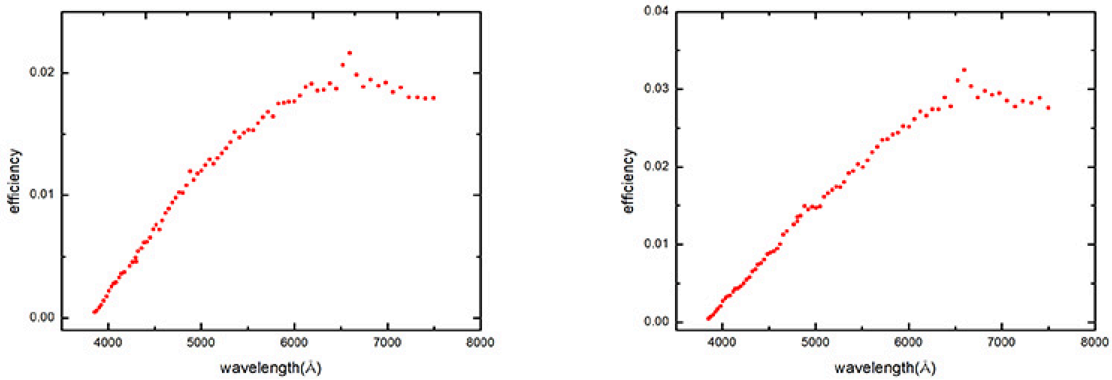

Fig. 8 Efficiency curve of HiRES with different fibers (*left*: fiber diameter of 1.2″, *right*: fiber diameter of 2.0″).

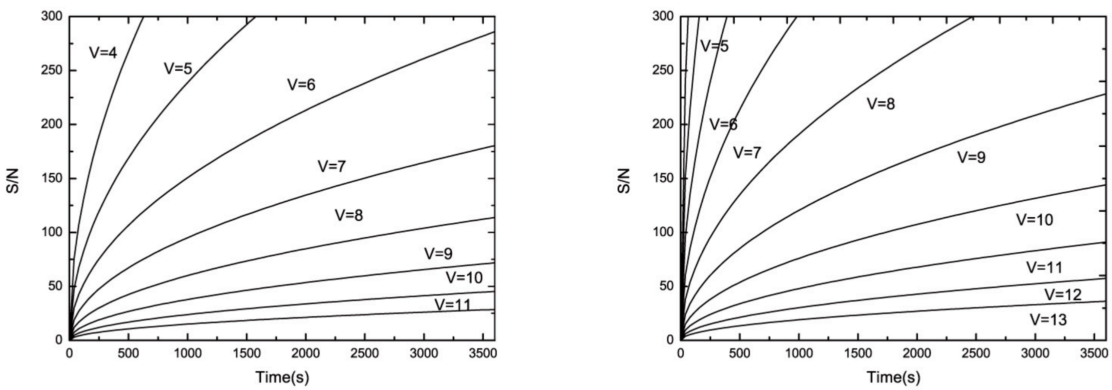

Fig. 9 The relation between S/N and exposure time for different magnitudes at 550 nm with different fibers (*left*: fiber diameter of 1.2″, *right*: fiber diameter of 2.0″).

3.2 Multicolor Photometric System

The multicolor photometric system consists of a PI VersArray 1300B CCD (PI CCD) camera and a set of standard Johnson/SDSS filters. PI CCD is a full-frame and back illuminated CCD produced by the Princeton Instruments company. It was the first scientific instrument operated on the Lijiang 2.4-meter telescope, and can be used for the common photometric and spectral observations. The major parameters of this CCD camera are listed in Table 5. The image scale of the PI CCD is 0.20″/pixel, which can match the photometric requirement of the telescope. The high quantum efficiency and low readout noise make it more suitable for photometric observation. Nowadays, the PI CCD is installed at one of the side ports as a backup photometric camera.

3.3 HiRES

HiRES is a high-resolution fiber spectrograph developed by Nanjing Institute of Astronomical Optics & Technology and Yunnan Observatories. It has been put into operation since November, 2015. The optical diagram of the spectrograph is shown in Figure 7. We can use HiRES to perform high-resolution spectral observation.

Most of the optical elements of HiRES are mounted on an independent optical platform placed in the spectral room at the grand floor outside of the dome. The spectral room can maintain very stable temperature ($28 \pm 0.25°$ C) and pressure (30 ± 1 Pa), in order to match the requirements of high-precision radial velocity observation. Two fibers have been installed on the Cassegrain part of the telescope. One fiber with a diameter of 2.0″ provides a spectral resolution of 32 000 at 550 nm. The other with a diameter of 1.2″ enables a spectral resolution of 49 000 at 550 nm. The wavelength coverage of HiRES is from 320 nm to 920 nm. Observers can choose a suitable fiber depending on the observation requirement and weather condition. There is also a photomultiplier tuber installed in HiRES to improve the pointing and focusing of telescope and to estimate the exposure time for the target. The CCD chip of HiRES is also produced by the e2v company. The chip is also back illuminated type and it is more sensitive in the blue-end. Detailed parameters of this CCD are listed in Table 6. HiRES relies on a Th-Ar lamp for wavelength calibration at present, and we will add iodine vapor as one reference to improve the

Table 7 Parameters of CCD for LiJET

Parameter	Value
Pixels	4096×4096
Pixel Size	15 μm×15 μm
Image Area	49.2 mm×49.2 mm
Cooling Mode	Cryogenic ∼−130° C
Gain	$1.37e^{-}$
Readout Noise	$11.0e^{-}$

accuracy of the calibration in the future. Limited by the star monitoring system, the observational limiting magnitude to use HiRES is 13 mag under the resolution of 32 000 with an 1800 second exposure at 550 nm and S/N ratio of about 10. The efficiency curve of the whole system is plotted in Figure 8. The relation between the S/N and the exposure time for different magnitudes at 550 nm with different fibers is displayed in Figure 9.

3.4 LiJET

LiJET is a fiber spectrograph that can provide high-precision radial velocity measurements. This instrument is especially designed for exoplanet observations, and it can be also advantageous for other high-resolution spectral observations (Ge et al. 2010). It has two observational modes. One is Direct Echelle Mode (DEM) mode, which has a resolution of 30 000 with the 1.0″ slit, and it covers the wavelength between 390 nm and 1000 nm. The other is Dispersed Fixed-Delay Interferometry (DFDI) mode or Radial Velocity Mode (RVM), which has a resolution of 18 000 with the 1.6″ slit, and it covers wavelengths between 390 nm and 690 nm with spectral order from 29 to 52. Under DFDI mode, the fixed delay interferometer is comprised of the medium-precision spectrograph to measure the stellar Doppler effect for exoplanet detection. The precision of the radial velocity calibration is 2.5 m s^{-1} under the DFDI mode. The optical structures of these two modes are depicted in Figure 10 and Figure 11. In order to detect the high-precision radial velocity, LiJET has high-precision temperature and pressure control. The temperature and pressure are very stable, which can achieve 0.1% precision of the variability. The parameters of the LiJET CCD are listed in Table 7.

3.5 CHILI

CHILI is based on a stock VIRUS unit developed for HETDEX. We can perform 2D spectral observations for extended sources with this instrument. The unit has two spectrograph channels with fixed angles between the collimator and camera. The fiber integral field unit (IFU) is mounted at its input. At the output, the fibers are arrayed into two linear arrays, each having 247 fibers. The IFU consists of 494 fibers with a core diameter of 200 microns. It is arranged in a hexagonal matrix at the input under a configuration with 23 rows of 11 or 12 fibers fed by micro-lens focal reducer optics. The FOV is 71″×76″. It can be fully filled with the observed sky region. The micro-lens fill factor is at least 95%, and it is not necessary to dither the telescope in order to fill in the observed sky region. The calibration source is Hg, Cd and Ne emission line lamps. The optical diagram and structure of CHILI are shown in Figure 12, and some key parameters are described in Table 8.

Table 8 Key Parameters Describing CHILI

CCD	Number of Pixels	2048×2048
	Pixel Size	15 μm×15 μm
Grating 1	Resolving Power	900 (350 nm–550 nm)
Grating 2	Resolving Power	900 (460 nm–720 nm)

3.6 Calibration

We routinely target dozens of flux standard stars during photometric nights and derive the average extinction curve for Lijiang Observatory. Table 9 lists all the Landolt standard stars that were observed on 2013 Nov. 6 and 7. The exposure time for each band is $U = 90$ s, $B = 30$ s, $V = 10$ s, $R = 10$ s, $I = 10$ s. All the CCD images were corrected for bias, flat field and cleaned of cosmic rays using IRAF. The results are shown in Figure 13. This plot was made by low-dispersion spectra (G3+Slit 10.0″) and $UBVRI$ filters with YFOSC.

Observations of the same targets on 2013 Nov. 6 and 7 can be used to obtain the S/N among UBVRI-bands in different photometric systems. Figure 14 displays the comparison between YFOSC and PI CCD among $UBVRI$-bands for the same targets. The S/N and magnitude in Figure 14 are defined by the following equations

$$\frac{\mathrm{S}}{\mathrm{N}} = \frac{N_{\rm star}}{\sqrt{N_{\rm star} + n_{\rm pix}(N_{\rm sky} + N_{\rm dark} + N^2_{\rm readout})}}, \quad (1)$$

$$\mathrm{Magnitude} = M_{\rm stand} + KX\,, \quad (2)$$

where $N_{\rm star}$ is the photons collected from targets; $N_{\rm sky}$ is the photons per pixel from the sky background; $N_{\rm dark}$ is the CCD dark current per pixel; $N_{\rm readout}$ is the readout noise; $n_{\rm pix}$ is the full width at half maximum (FWHM) of each target; $M_{\rm stand}$ is magnitude in the Landolt photometry system for the targets; K is the extinction coefficient and X is the airmass. For YFOSC and PI CCD, the readout noise is estimated well and the dark current is negligible. Generally, YFOSC has higher S/N than PI CCD, especially in U and I bands.

The same observational data can also be used to estimate the efficiency of the photometric system in $UBVRI$-

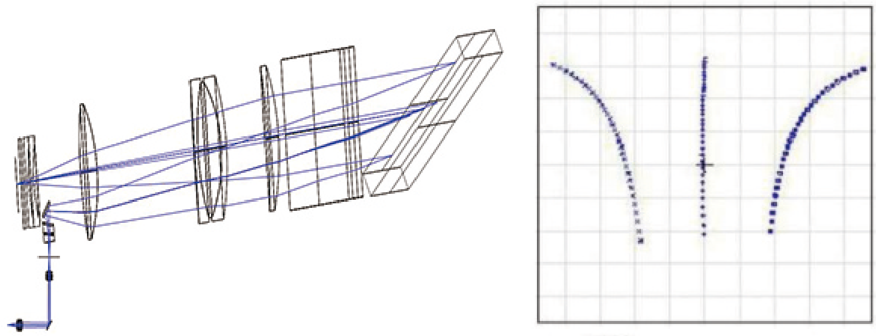

Fig. 10 Layout of the DEM mode (*left*) and spectra format on the CCD (*right*).

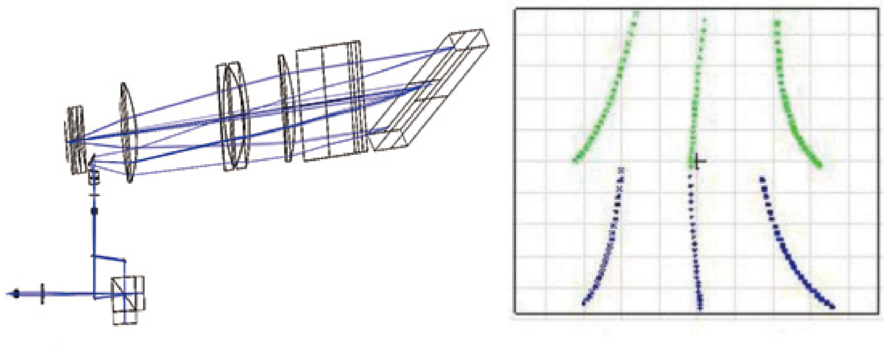

Fig. 11 Layout of RVM (*left*) and spectra format on the CCD (*right*).

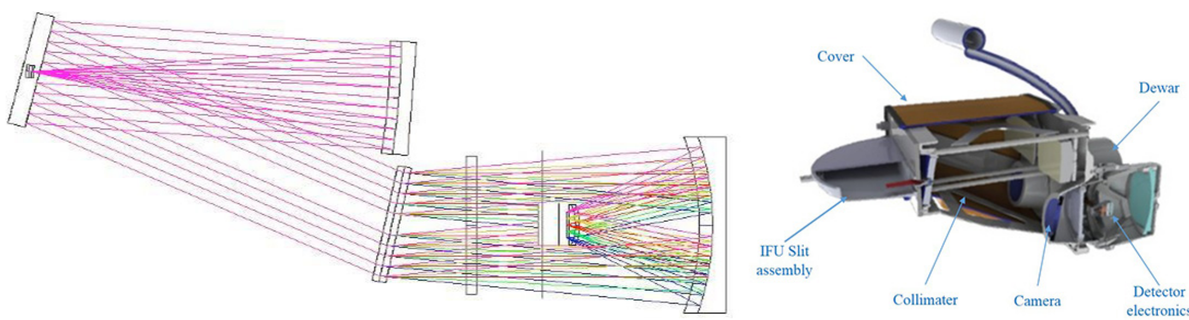

Fig. 12 The optical diagram and structure of CHILI.

bands. Table 10 gives the efficiencies from the telescope to the CCD for YFOSC and PI CCD at two epochs, respectively. The throughput estimated in January and November implies the throughput of the telescope decreased. It also suggests the effect of mirror re-coating.

4 AUXILIARY EQUIPMENT

4.1 Dome

The dome of the 2.4-meter telescope is a classical-type design with shutters that can open and close during observations. The main purpose for applying this type of dome is to prevent the influence from wind. In order to improve the dome seeing, there are eight side windows and four air channels that balance the temperature inside and outside the dome. There is an independent PLC system that can communicate with the MCC and receive the control request from the TCC to open/close the shutter and to track the target along with the telescope.

The dome is a super-hemisphere sphere with a steel welded spherical grid structure. The dome mainly consists of eight parts, including chassis, arched girder, beams, shutter, shutter driver, azimuth driver, electric control system and a crane inside. The dome skeleton is formed by

Table 9 Landolt Standard Stars Used in this Paper

Star	α(J2000)	δ(J2000)	V	$U-B$	$B-V$	$V-R$	$V-I$
SA92_245	00:54:16	+00:39:51	13.818	1.418	1.189	1.189	1.836
SA92_248	00:54:31	+00:40:15	15.346	1.128	1.289	1.289	1.243
SA92_249	00:54:34	+00:41:05	14.325	0.699	0.24	0.24	0.769
SA92_250	00:54:37	+00:38:56	13.178	0.814	0.48	0.48	0.840
SA92_425	00:55:59	+00:52:58	13.941	1.191	1.173	1.173	1.382
SA92_426	00:56:00	+00:52:53	14.466	0.729	0.184	0.184	0.808
SA92_355	00:56:06	+00:50:47	14.965	1.164	1.201	1.201	1.404
SA92_430	00:56:16	+00:53:16	14.440	0.567	–0.04	–0.04	0.676
SA95_330	03:54:31	+00:29:05	12.174	1.999	2.233	2.233	2.266
SA95_275	03:54:44	+00:27:20	13.479	1.763	1.74	1.74	1.942
SA95_276	03:54:46	+00:27:20	14.118	1.225	1.218	1.218	1.394
SA95_112	03:53:40	−00:01:13	15.502	0.662	0.077	0.077	1.225
SA95_41	03:53:41	−00:02:31	14.06	0.903	0.297	0.297	1.174
SA95_42	03:53:44	−00:04:33	15.606	–0.215	–1.111	–1.111	–0.299
SA95_115	03:53:44	−00:00:48	14.680	0.836	0.096	0.096	1.156
SA95_43	03:53:49	−00:03:01	10.803	0.51	–0.016	–0.016	0.624
SA92_410	00:55:15	+01:01:49	14.984	0.398	–0.134	–0.134	0.481
SA92_412	00:55:16	+01:01:53	15.036	0.457	–0.152	–0.152	0.589
SA95_328	03:54:19	+00:36:28	13.525	1.532	1.298	1.298	1.776
SA95_329	03:54:24	+00:37:07	14.617	1.184	1.093	1.093	1.408

welded angle steel, and the arched girder is welded to the 12 mm steel plate. The steel channel can guarantee the stiffness requirement of the dome and can also be used as the foundation support for the crane. The open range of the shutter is from –3° to 100° by implementing a fixed chain driver. It has dual protection by relying on an electrical-limiting switch and mechanical-limiting instruments. The chassis of the dome uses a wheel rail structure. It is driven by electrical motors with a decelerating gear, and it can move the dome 360° along the azimuth.

4.2 Coating Machine

The coating machine (ZZS3200) is developed by Yunnan Observatories and the Chengdu Institute of Optical and Electronic Technology. It is used for the 2.4-meter telescope and 1.8-meter telescope in Lijiang Observatory. The inner diameter of the machine is 3200 mm, and the height of the machine is 3500 mm. It is divided into two parts. The lower part is mounted on the rail that can move out to put a mirror on it. We re-coated the primary mirror of the 2.4-meter telescope using this coating machine in October 2012, and the optical efficiency was increased significantly. Comparison of the same target before and after the re-coating is shown in Table 11. We re-coat the primary mirror of the 2.4-meter telescope every 2 years in order to maintain excellent optical efficiency.

4.3 Astronomical Site Monitoring System

The Astronomical Site Monitoring System (ASMS) is a system that monitors the weather conditions, astronomical conditions and instruments at the site. The system can provide information like weather, seeing conditions, clouds, all-sky image and so on. Moreover, it can also send

Table 10 Efficiency from telescope to CCD of PICCD and YFOSC in $UBVRI$

Filter	PICCD (%)	YFOSC (%)	Ratio (YF/PI)
		Jan. 2013	
U	3.9±0.2	8.9±0.5	2.27
B	12.5±0.3	15.3±0.4	1.23
V	22.4±0.4	22.5±0.3	1.01
R	21.2±0.3	20.3±0.4	0.96
I	17.1±0.4	34.5±0.5	2.02
		Nov. 2013	
U	3.2±0.3	7.3±0.4	2.29
B	10.0±0.4	12.4±0.4	1.24
V	18.3±0.3	18.0±0.3	0.98
R	17.2±0.3	16.3±0.4	0.96
I	13.8±0.4	28.1±0.4	2.03

Table 11 Comparison of Same Target before and after Re-coating

	Before (ADU)	After (ADU)
Observing Time	2011–12–20 BT19:32:30	2012–12–13 BT 19:53:33
PG2331+055	173888	355453
PG2331+055A	1203000	2377830
PG2331+055B	259466	503664

weather data to the TCS for protecting the telescope and can add weather information to the head of observation data files to help in data processing. This system consists of a weather station and monitoring system. It can be accessed through the internet[1].

5 SCIENTIFIC ACHIEVEMENT

Many scientific results have been obtained from the Lijiang 2.4-meter telescope. For example, with the low-dispersion spectrograph of YFOSC, Wu et al. (2015) identified the highest luminosity quasar in the early universe ($z\sim6.3$)

[1] `http://weather.gmg.org.cn:9000`

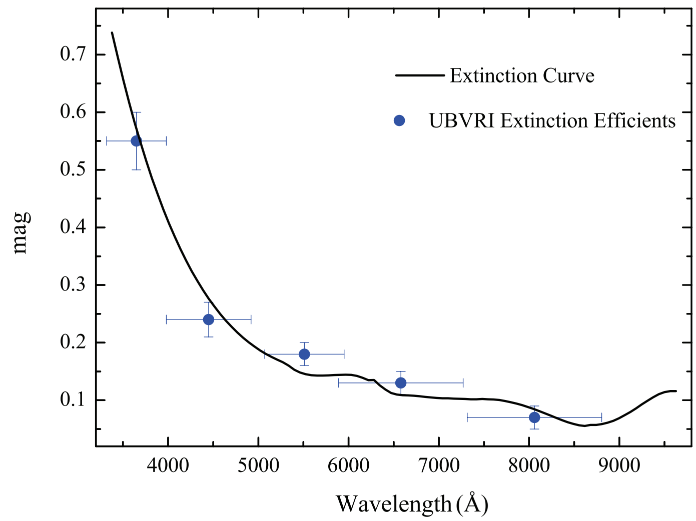

Fig. 13 Average atmospheric extinction curve and coefficients at Lijiang observatory. The curve was obtained by YFOSC long-slit spectrograph and overplotted with coefficients of $UBVRI$-bands photometry. The horizontal error bars of coefficients stand for the FWHM of the filters and vertical error bars for the measurement error.

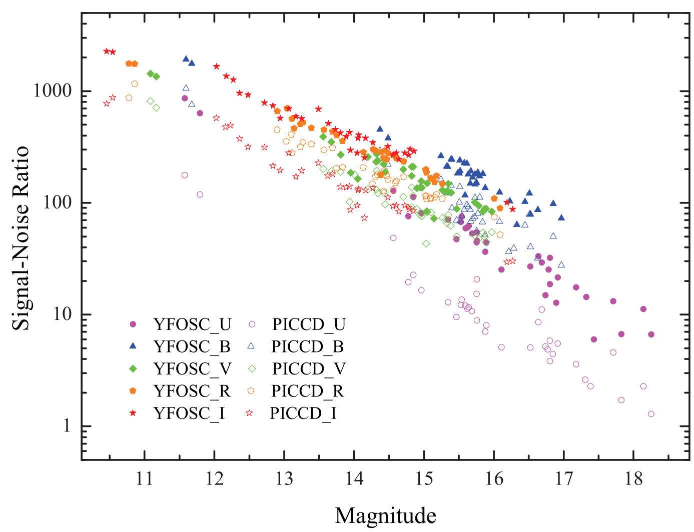

Fig. 14 S/N comparisons between YFOSC and PI CCD among $UBVRI$ bands.

found to date. The ultra-high luminosity of this quasar indicates that there may be a 12 billion solar-mass black hole in its core. This black hole is a magnitude bigger than others found before. How could a black hole with such mass have formed less than 1 billion years after the birth of the universe? This discovery raises new questions about the evolution of black holes and even the evolution of the universe.

By using YFOSC, Wang et al. (2014), Du et al. (2014, 2015, 2016b,a), Lu et al. (2016) and Li et al. (2016) performed reverberation-mapping observations of some high accretion rate AGNs. They measured the masses of a set of high accretion rate black holes, in order to study high-redshift cosmology.

Hundreds of observations targeting supernovae have been performed with this telescope in the past five years based on the Li-Jiang One hour per Night observation of Supernovae (LiONS) project. This project focuses on type Ia supernovae at a very early phase or any peculiar events related to supernovae, and can monitor interesting targets with low-resolution spectroscopy and multi-band photometry immediately and frequently (e.g., Arcavi et al. 2017; Huang et al. 2015, 2016; Li et al. 2018; Liu et al. 2015; Zhai et al. 2016; Zhang et al. 2014a,b, 2016a, 2018a).

Some studies focus on intergalactic objects. Qian et al. (2015) carried out an optical variation study of a binary star using the 2.4-meter telescope. They found the first stable red dwarf binary. Qian et al. (2011) discovered one exoplanet that is orbiting an evolving binary star. Su et al. (2014) measured some stellar parameters for the study of white dwarfs.

Gamma-ray burst follow-up observation is also performed by the Lijiang 2.4-meter telescope. Mao et al. (2012) studied the GRB 100219A optical afterglow. We also collected observations for the electromagnetic counterparts of gravitational waves in cooperation with astronomers around the world.

6 SUMMARY AND FUTURE EXPECTATION

The Lijiang 2.4-meter telescope is the largest optical telescope at present in China for general astronomical observation. After 10 years of operation, it has been equipped with many kinds of observational instruments covering photometry, low/medium resolution spectral, and high-resolution spectral and two-dimensional spectral observation. Many kinds of scientific research can be performed by this telescope, and a set of scientific achievements have been obtained. More than 190 papers related to the Lijiang 2.4-meter telescope have been published.

Apart from the instruments described above, there are two new instruments under construction. One is the EMCCD used for both high precision temporal observation and high-spatial resolution photometry with lucky imaging techniques. The other is the near-infrared spectrograph (ONICE) utilized for infrared spectral observation. Moreover, observers can also install their own specified instruments onto the Cassegrain side port with the interface plate provided. By applying these new instruments, the Lijiang 2.4-meter telescope can be involved in more and more scientific research topics. It will play a more unique role in observational astronomy in the future.

Acknowledgements We thank all the present and former staffs at Lijiang Observatory for their effort at installing, operating and maintaining the Lijiang 2.4-meter telescope, and the staffs who help to develop the instruments. This work is supported by the Joint Research Fund in Astronomy (U1631127, U1631129 and U1831204) under cooperative agreement between the National Natural Science Foundation of China (NSFC) and Chinese Academy of Sciences (CAS), the National Natural Science Foundation of China (NSFC) (11473068, 11603072 and 11573067), the National Key R&D Program of China (2018YFA0404603), and also supported by the Key Laboratory for the Structure and Evolution of Celestial Objects, Chinese Academy of Sciences (CAS).

References

Arcavi, I., Howell, D. A., Kasen, D., et al. 2017, Nature, 551, 210
Du, P., Hu, C., Lu, K.-X., et al. 2014, ApJ, 782, 45
Du, P., Hu, C., Lu, K.-X., et al. 2015, ApJ, 806, 22
Du, P., Lu, K.-X., Zhang, Z.-X., et al. 2016a, ApJ, 825, 126
Du, P., Lu, K.-X., Hu, C., et al. 2016b, ApJ, 820, 27
Fan, Y.-F., Bai, J.-M., Zhang, J.-J., et al. 2015, RAA (Research in Astronomy and Astrophysics), 15, 918
Ge, J., Chang, L., Groot, J., et al. 2010, in American Astronomical Society Meeting Abstracts, 215, 348.03
Huang, F., Wang, X., Zhang, J., et al. 2015, ApJ, 807, 59
Huang, F., Wang, X., Zampieri, L., et al. 2016, ApJ, 832, 139
Li, Y.-R., Wang, J.-M., Ho, L. C., et al. 2016, ApJ, 822, 4
Li, L., Wang, X., Zhang, J., et al. 2018, MNRAS, 478, 4575
Liu, Z.-W., Zhang, J.-J., Ciabattari, F., et al. 2015, MNRAS, 452, 838
Lu, K.-X., Du, P., Hu, C., et al. 2016, ApJ, 827, 118
Lun, B.-L., Qin, S.-N., Wang, J.-G., et al. 2014, Astronomical Research and Technology, 11, 176
Mao, J., Malesani, D., D'Avanzo, P., et al. 2012, A&A, 538, A1
Qian, S.-B., Liu, L., Liao, W.-P., et al. 2011, MNRAS, 414, L16
Qian, S.-B., Jiang, L.-Q., Fernández Lajús, E., et al. 2015, ApJ, 798, L42
Su, J., Li, Y., Fu, J.-N., & Li, C. 2014, MNRAS, 437, 2566
Wang, J.-M., Du, P., Hu, C., et al. 2014, ApJ, 793, 108
Wu, X.-B., Wang, F., Fan, X., et al. 2015, Nature, 518, 512
Xin, Y.-X., Wang, C.-J., Fan, Y.-F., et al. 2017, Progress in Astronomy, 35, 367
Zhai, Q., Zhang, J.-J., Wang, X.-F., et al. 2016, AJ, 151, 125
Zhang, J.-J., Fan, Y.-F., Chang, L., et al. 2012, Astronomical Research and Technology, 9, 411
Zhang, J.-J., Wang, X.-F., Bai, J.-M., et al. 2014a, AJ, 148, 1
Zhang, J., Wang, X., Mazzali, P. A., et al. 2014b, ApJ, 797, 5
Zhang, J.-J., Wang, X.-F., Sasdelli, M., et al. 2016a, ApJ, 817, 114
Zhang, K., Wang, X., Zhang, J., et al. 2016b, ApJ, 820, 67
Zhang, J., Wang, X., Vinkó, J., et al. 2018a, ApJ, 863, 109
Zhang, K., Wang, X., Zhang, J., et al. 2018b, MNRAS, 481, 878